



## Dopant activation in Sn-doped Ga<sub>2</sub>O<sub>3</sub> investigated by X-ray absorption spectroscopy

S. C. Siah, R. E. Brandt, K. Lim, L. T. Schelhas, R. Jaramillo, M. D. Heinemann, D. Chua, J. Wright, J. D. Perkins, C. U. Segre, R. G. Gordon, M. F. Toney, and T. Buonassisi

Citation: *Applied Physics Letters* **107**, 252103 (2015); doi: 10.1063/1.4938123

View online: <http://dx.doi.org/10.1063/1.4938123>

View Table of Contents: <http://scitation.aip.org/content/aip/journal/apl/107/25?ver=pdfcov>

Published by the AIP Publishing

---

### Articles you may be interested in

Oxygen deficiency and Sn doping of amorphous Ga<sub>2</sub>O<sub>3</sub>  
*Appl. Phys. Lett.* **108**, 022107 (2016); 10.1063/1.4938473

Experimental and theoretical investigation of the electronic structure of Cu<sub>2</sub>O and CuO thin films on Cu(110) using x-ray photoelectron and absorption spectroscopy  
*J. Chem. Phys.* **138**, 024704 (2013); 10.1063/1.4773583

Ge doped HfO<sub>2</sub> thin films investigated by x-ray absorption spectroscopy  
*J. Vac. Sci. Technol. A* **28**, 693 (2010); 10.1116/1.3430562

Electronic structure of oxidized Ni/Au contacts on p- GaN investigated by x-ray absorption spectroscopy  
*Appl. Phys. Lett.* **78**, 2718 (2001); 10.1063/1.1370121

Local microstructures of Si in GaN studied by x-ray absorption spectroscopy  
*Appl. Phys. Lett.* **75**, 534 (1999); 10.1063/1.124439

---

The advertisement features a stylized circuit diagram with nodes labeled 'COMPUTING', 'ENGINEERING', and 'SCIENCE'. A purple line representing a circuit path leads from the 'SCIENCE' node to a laboratory flask containing a blue liquid. On the left, there is a small image of the 'Computing in Science and Engineering' (CiSE) magazine cover, which includes the text 'CITIZEN SCIENCE' and the IEEE logo. Below the diagram, the text reads: 'CiSE magazine is an innovative blend.'

## Dopant activation in Sn-doped Ga<sub>2</sub>O<sub>3</sub> investigated by X-ray absorption spectroscopy

S. C. Siah,<sup>1,a)</sup> R. E. Brandt,<sup>1</sup> K. Lim,<sup>2,3</sup> L. T. Schelhas,<sup>2</sup> R. Jaramillo,<sup>1</sup> M. D. Heinemann,<sup>4</sup> D. Chua,<sup>5</sup> J. Wright,<sup>6</sup> J. D. Perkins,<sup>7</sup> C. U. Segre,<sup>6</sup> R. G. Gordon,<sup>5</sup> M. F. Toney,<sup>2</sup> and T. Buonassisi<sup>1,b)</sup>

<sup>1</sup>Massachusetts Institute of Technology, Cambridge, Massachusetts 02139, USA

<sup>2</sup>SLAC National Accelerator Laboratory, Stanford Synchrotron Radiation Lightsource, Menlo Park, California 94025, USA

<sup>3</sup>Department of Materials Science and Engineering, Stanford University, Stanford, California 94305, USA

<sup>4</sup>PVcomB, Helmholtz-Zentrum Berlin, 12489 Berlin, Germany

<sup>5</sup>Department of Chemistry Materials Science and Chemical Biology, Harvard University, Cambridge, Massachusetts 02138, USA

<sup>6</sup>Physics Department and CSRR, Illinois Institute of Technology, Chicago, Illinois 60616, USA

<sup>7</sup>National Renewable Energy Laboratory, Golden, Colorado 80401, USA

(Received 20 June 2015; accepted 5 December 2015; published online 23 December 2015)

Doping activity in both beta-phase ( $\beta$ -) and amorphous (a-) Sn-doped gallium oxide (Ga<sub>2</sub>O<sub>3</sub>:Sn) is investigated by X-ray absorption spectroscopy (XAS). A single crystal of  $\beta$ -Ga<sub>2</sub>O<sub>3</sub>:Sn grown using edge-defined film-fed growth at 1725 °C is compared with amorphous Ga<sub>2</sub>O<sub>3</sub>:Sn films deposited at low temperature (<300 °C). Our XAS analyses indicate that activated Sn dopant atoms in conductive single crystal  $\beta$ -Ga<sub>2</sub>O<sub>3</sub>:Sn are present as Sn<sup>4+</sup>, preferentially substituting for Ga at the octahedral site, as predicted by theoretical calculations. In contrast, inactive Sn atoms in resistive a-Ga<sub>2</sub>O<sub>3</sub>:Sn are present in either +2 or +4 charge states depending on growth conditions. These observations suggest the importance of growing Ga<sub>2</sub>O<sub>3</sub>:Sn at high temperature to obtain a crystalline phase and controlling the oxidation state of Sn during growth to achieve dopant activation.

© 2015 AIP Publishing LLC. [<http://dx.doi.org/10.1063/1.4938123>]

Many optoelectronic devices incorporate a transparent conducting oxide (TCO) to transport charge carriers and photons to and from active semiconductor layers. An outstanding material challenge is to develop a wide-bandgap TCO with both small electron affinity and high donor concentration (Fermi energy), enabling a low-loss electron-selective contact for emerging materials with high conduction-band energies, including GaN, Cu<sub>2</sub>O, and *n*-type silicon.

For this purpose, beta-phase gallium oxide ( $\beta$ -Ga<sub>2</sub>O<sub>3</sub>) has recently emerged as a promising candidate TCO. With an electron affinity of 3.7 eV,<sup>1</sup> bandgap of 4.8 eV (Ref. 2) and transmissivity above 80% in the wavelength range of 300–1000 nm,<sup>3</sup> Ga<sub>2</sub>O<sub>3</sub> appears to be an excellent candidate wide-bandgap TCO with low electron affinity. Ga<sub>2</sub>O<sub>3</sub> can be doped with tin, achieving donor concentrations above 10<sup>19</sup> cm<sup>-3</sup> when grown in bulk-crystal form<sup>3</sup> and above 10<sup>18</sup> cm<sup>-3</sup> when deposited by molecular-beam epitaxy (MBE) in the 540–600 °C range.<sup>4</sup> However, thin films deposited using atomic-layer deposition (ALD) and pulsed-laser deposition (PLD) at more moderate temperatures in the 100–200 °C range have not exhibited high Sn dopant activation; as observed in this work, these films are typically highly resistive, even with a concentration of 10<sup>20</sup> cm<sup>-3</sup> Sn dopants. Identifying a means to achieve higher Sn dopant activation in low-temperature ALD- or PLD-deposited films could increase the industrial relevance of Ga<sub>2</sub>O<sub>3</sub>:Sn for cost-

sensitive applications including field-effect transistors,<sup>4</sup> solar cells,<sup>5–7</sup> gas sensors,<sup>8</sup> and lasers.<sup>9</sup> Determining the chemical states of active and inactive Sn dopants in Ga<sub>2</sub>O<sub>3</sub> is a first and necessary step toward developing intuition and theory to guide thin-film synthesis.

Herein, the chemical state of Sn dopants in  $\beta$ -Ga<sub>2</sub>O<sub>3</sub> bulk crystals and amorphous (a-)Ga<sub>2</sub>O<sub>3</sub> thin films deposited by ALD and PLD is investigated. Synchrotron-based X-ray absorption spectroscopy (XAS), a probe of local atomic structure and chemical state, is employed to define requirements for successful dopant activation. It is found that Sn dopant activation correlates with Sn chemical state and Ga<sub>2</sub>O<sub>3</sub> matrix crystallinity. The local structures of the metal cations in these different samples provide insights into how dopant atoms are incorporated into the host Ga<sub>2</sub>O<sub>3</sub> lattices and govern electrical conductivity.

$\beta$ -Ga<sub>2</sub>O<sub>3</sub>:Sn single crystal (SC) is purchased commercially from Tamura Corporation and is grown from the melt using the edge-defined film-fed growth (EFG) method.<sup>4</sup> In addition, a-Ga<sub>2</sub>O<sub>3</sub>:Sn thin films are deposited using ALD and PLD methods. The ALD film is deposited at 120 °C in a custom-built cylindrical reactor with a 30 cm long and 3 cm wide sample stage, and a chamber volume of 0.627 l. The Ga and Sn precursors used in the ALD process are bis( $\mu$ -dimethylamino)tetrakis(dimethylamino)digallium<sup>6,10</sup> and tetrakis(dimethylamido)tin(IV), respectively. The oxygen source is H<sub>2</sub>O. During the ALD process, the temperatures of the Ga and Sn precursors are maintained at 120 and 60 °C, respectively, while H<sub>2</sub>O is kept at 25 °C. High-purity N<sub>2</sub> is used as a carrier gas, and the exposures of the gallium

<sup>a)</sup>Electronic mail: [sincheng@alum.mit.edu](mailto:sincheng@alum.mit.edu)

<sup>b)</sup>Electronic mail: [buonassisi@mit.edu](mailto:buonassisi@mit.edu)

and tin precursors and  $\text{H}_2\text{O}$  are estimated to be approximately 3, 2 and 5 Torr seconds, respectively. The  $\text{Ga}_2\text{O}_3:\text{Sn}$  films are deposited on Si/SiO<sub>2</sub> substrates by repeating a supercycle consisting of 19-times subcycle of  $\text{Ga}_2\text{O}_3$  (bis( $\mu$ -dimethylamino)tetrakis(dimethylamino)digallium/purge/ $\text{H}_2\text{O}$ /purge) followed by 1 time subcycle of  $\text{SnO}_2$  (tetrakis(dimethylamido)tin(IV)/purge/ $\text{H}_2\text{O}$ /purge). Purge time is set to be 30 s. The deposition rate is measured to be  $\sim 0.2$  nm per subcycle. The PLD film is deposited on quartz substrate using  $\text{Ga}_2\text{O}_3$  and  $\text{SnO}_2$  targets, and the energy density of the pulsed KrF excimer laser (248 nm) is set to 300 mJ with a repetition rate of 10 Hz and a distance of 10 cm between the target and the sample substrate. The substrate is rotated during the 50 laser pulses applied to the  $\text{Ga}_2\text{O}_3$  target and kept at a fixed angle during 2 pulses applied to the  $\text{SnO}_2$  target. This procedure is repeated 400 times, resulting in a homogeneous  $\text{Ga}_2\text{O}_3$  film with a Sn doping gradient across the sample from approximately 1 at. % to 4 at. %. The oxygen partial pressure is set to 100  $\mu$ Torr for the depositions at 400 °C to ensure that the film is close to stoichiometric. The deposition temperature for PLD films is chosen to be 400 °C to ensure mixing of Ga and Sn atoms, and the deposition temperature for ALD films is chosen to be lower at 120 °C as the Ga precursor decomposes above 500 °C. The thickness of both the ALD and PLD films are about 200 nm, and no postannealing is performed for both ALD and PLD samples. For the PLD samples, the in-depth homogeneity of Ga along the substrate corresponds to approximately 0.5 nm of  $\text{Ga}_2\text{O}_3$  deposited between the Sn pulses and the [Sn] homogeneity along the substrate is between 1% and 4% along a 2 in. substrate. However, spatial homogeneity is insignificant in this work as the characterization techniques involved have beam spot sizes that are  $< 2 \times 2$  mm<sup>2</sup>.

The stoichiometry of the ALD and PLD thin films are measured using Rutherford Backscattering Spectroscopy (RBS) and determined to be  $\text{Ga}_2\text{O}_{3.41}\text{Sn}_{0.065}$  and  $\text{Ga}_2\text{O}_{2.91}\text{Sn}_{0.072}$  respectively. Accordingly, the atomic concentrations of Sn for ALD and PLD thin films are estimated to be  $2.3 \times 10^{20}$  and  $2.9 \times 10^{20}$  cm<sup>-3</sup>, respectively. The atomic concentrations of Sn for a set of SC samples is obtained from Tamura Corporation for comparison. In addition, the net carrier density for SC  $\text{Ga}_2\text{O}_3:\text{Sn}$  samples determined by electrochemical capacitance-voltage (ECV) are also obtained from Tamura Corporation. Hall and four-point probe measurements are performed for all the samples using a  $\text{Ga}_2\text{O}_3:\text{Sn}/\text{Ti}$  (100 nm)/Au (100 nm) stack for ohmic contact<sup>11</sup> but only the SC  $\text{Ga}_2\text{O}_3:\text{Sn}$  sample exhibits detectable signals. The Hall mobility and net carrier density ( $N_D - N_A$ ) of the SC are determined to be 110 cm<sup>2</sup>/V s and  $4 \times 10^{18}$  cm<sup>-3</sup> ( $N_D - N_A$  by ECV =  $7 \times 10^{18}$  cm<sup>-3</sup>), respectively. The ALD and PLD film structures are also analyzed with wide angle X-ray diffraction (XRD) on Beamline 11-3 at the Stanford Synchrotron Radiation Lightsource (SSRL). Two-dimensional scattering is collected with a MAR345 image plate at grazing incidence at an incident energy of 12.7 keV. Spectra are integrated between  $5^\circ < \phi < 175^\circ$  using the GSAS II analysis software. The resistivities for our ALD and PLD samples are estimated to be  $> 2000 \Omega$  cm based on the detection limit of the four-point probe system. By assuming a mobility of  $> 0.1$  cm<sup>2</sup>/V s, the upper limit of

carrier density is estimated to be  $3.0 \times 10^{16}$  cm<sup>-3</sup> for our a- $\text{Ga}_2\text{O}_3:\text{Sn}$  films. Figure 1 compares the net carrier density of the SC samples as a function of Sn concentration. It can be observed that the SC samples grown via EFG have an activation ratio close to 100%. In comparison, the Sn dopant atoms in our ALD and PLD deposited films are either largely unactivated or highly compensated, as evident through their high resistivities and low carrier concentrations.

We perform Ga *K*-edge XAS at Beamline 4-3 of the Stanford Synchrotron Radiation Lightsource and Sn *K*-edge XAS at MRCAT Beamline 10-ID of the Advanced Photon Source. In both measurements, the thin-film samples are measured in fluorescence mode with an incident beam of approximately  $500 \times 500 \mu\text{m}^2$ . The *K*-edge fluorescence for Ga and Sn is measured by a Lytle detector and silicon Vortex solid-state detector, respectively. Reference metallic Ga or Sn thin-foils are measured to account for relative energy drifts. The X-ray absorption near-edge structures (XANES) and extended X-ray absorption fine structures (EXAFS) are isolated by normalizing the absorption spectrum and subtracting the smooth atomic background absorption signal from the measured absorption signal using the AUTOBK algorithm in Athena with  $R_{\text{bkg}} = 1.0 \text{ \AA}$ .<sup>12-14</sup> After background removal, the processed data are transformed from energy space to *k*-space using the relationship,  $k^2 = 2m(E - E_0)/\hbar^2$ , where *k* is the electron wavenumber, *m* is the electron mass,  $E_0$  is the *K*-edge absorption energy of the respective elements, and  $\hbar$  is Planck's constant. The spectra are weighted by  $k^2$  to compensate for amplitude decay. For further analysis, the  $k^2$ -weighted spectra data are Fourier-transformed with a Hanning window as a bandpass filter to enhance the signal to noise ratio within windows between  $k = 1.5$  and  $10.0 \text{ \AA}^{-1}$ .

The chemical states of Sn for each sample can be derived by comparing, in Figure 2, the respective XANES spectra with Sn metal foil, SnO powder, and SnO<sub>2</sub> powder references. The full XANES spectra are given in Figure S1.<sup>15</sup> The relative chemical shifts observed in the XANES spectra are due to changes in oxidation state, which alters the binding energy for electrons in the first shell.<sup>16</sup> Figure 2 shows that the average charge states of Sn atoms in our SC and ALD samples are similar to that of SnO<sub>2</sub> (Sn<sup>4+</sup>).

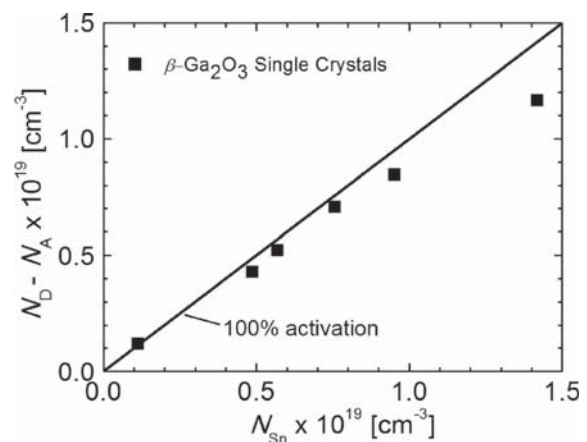


FIG. 1. Net carrier density of  $\beta\text{-Ga}_2\text{O}_3:\text{Sn}$  single crystals as a function of varying [Sn].

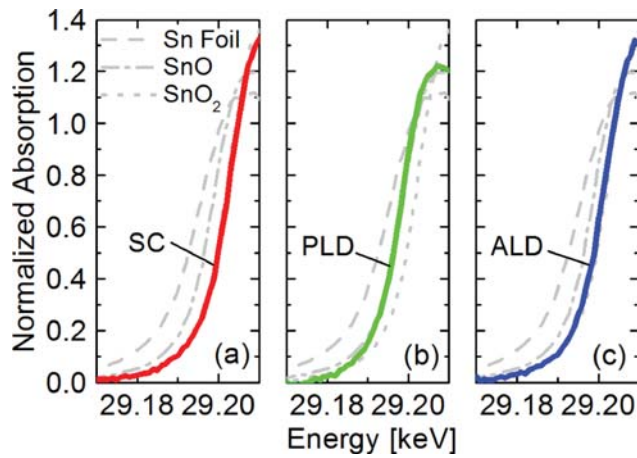


FIG. 2. Sn edge XANES spectra for (a) SC  $\beta$ -Ga<sub>2</sub>O<sub>3</sub>:Sn, (b) PLD a-Ga<sub>2</sub>O<sub>3</sub>:Sn, and (c) ALD a-Ga<sub>2</sub>O<sub>3</sub>:Sn samples. The dashed, dashed-dotted, and dotted lines represent Sn(0) metal (dashed-line), Sn(II)O (dashed-dotted line), and Sn(IV)O<sub>2</sub> (dotted line) references, respectively.

Comparing this with the resistivity data suggests that Sn<sup>4+</sup> can function as an electron donor under the correct conditions. However, its presence does not always result in free electrons due to other reasons including the formation of compensating defects or formation of secondary phases. The average oxidation state in our PLD sample corresponds to Sn<sup>2+</sup> (SnO), which is not likely to act as an electron donor. The presence of this reduced state (compared to the SC and ALD) suggests that the growth environment could be too reducing relative to the ALD and SC growth processes.

Next, EXAFS is used to investigate the structural origin of Sn doping. Figure 3 shows the Fourier-transformed spectra plotted as the magnitude,  $|\chi(R)|$ , for both the Ga and Sn *K*-edges. The first large peak in the  $|\chi(R)|$  spectrum is due to only single-scattering paths from the first nearest neighbor (1NN) shell of atoms, and higher-order peaks are due to single- and multiple-scattering paths involving neighboring atoms in 1NN and higher order shells. In both sets of spectra, the amplitudes of  $|\chi(R)|$  from higher-order shells ( $R > 2 \text{ \AA}$ ) for the ALD and PLD deposited samples are strongly attenuated, showing limited structural order beyond 1NN. The lack of long-range order is consistent with the amorphous

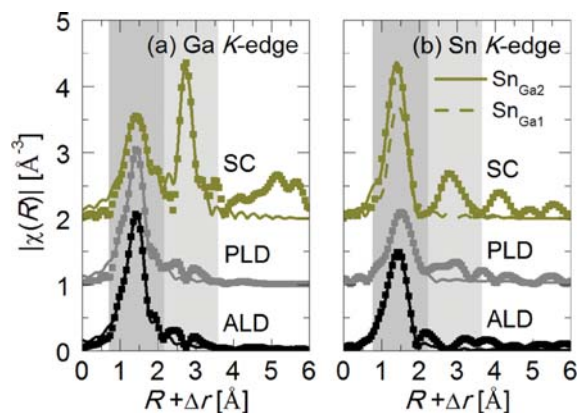


FIG. 3. Fourier-transformed EXAFS spectra plotted as the magnitude,  $|\chi(R)|$ , for (a) Ga and (b) Sn *K*-edges. The dark and light grey regions represent the first and second shell fitting windows for the SC sample at the Sn *K*-edge. Note the poor fit for Sn on the Ga1 site for the SC sample.

structure as characterized by our XRD measurements, as shown in supplementary Figure S2.<sup>15</sup>

To gain quantitative local structural information, the peaks are isolated and fitted using the EXAFS equation given by<sup>17</sup>

$$\chi(k) = S_0^2 \sum_j \frac{N_j f_j(k)}{k R_j^2} e^{-2k^2 \sigma_j^2} e^{-2R_j/\lambda(k)} \sin(2kR_j + \delta_j(k)), \quad (1)$$

where  $j$  indicates shells of like atoms,  $S_0^2$  is the passive electron reduction factor,  $N_j$  is the coordination number of atoms in the  $j$ th shell,  $k$  is the photoelectron wavenumber,  $R_j$  is the half path length,  $\sigma_j^2$  is the Debye-Waller factor or the mean-squared disorder of neighbor distance, and  $\lambda(k)$  is the electron mean free path. The scattering amplitude,  $f_j(k)$ , and the phase shift,  $\delta_j(k)$ , are dependent on the atomic number of the scattering atoms.  $S_0^2$  for both Ga (1.00) and Sn (1.14) are determined by fitting the crystalline Ga<sub>2</sub>O<sub>3</sub>:Sn SC sample and used as constants for other samples. The other fitting parameters for each scattering path are the changes in the half path length ( $\Delta R_{\text{eff}}$ ),  $\sigma_j^2$  and energy shift ( $\Delta E_0$ ). For the SC sample, the spectra are fitted up to the second-order peak, and the scattering paths used in the data fitting routines are calculated using the crystal structure of  $\beta$ -Ga<sub>2</sub>O<sub>3</sub>:Sn (space group C12/m1)<sup>18,19</sup> as a starting input into the ATOMS and FEFF6 codes implemented in Artemis.<sup>20</sup> In the unit cell of  $\beta$ -Ga<sub>2</sub>O<sub>3</sub>, there are two crystallographically nonequivalent Ga atoms (tetrahedral Ga1 and octahedral Ga2) and three nonequivalent O atoms (O1, O2, and O3). The Ga *K*-edge spectrum for the SC sample is modeled by considering equal contributions from the Ga1 and Ga2 sites,<sup>21</sup> and the Sn *K*-edge spectrum is fitted by considering either substitutional Sn-on-Ga1 (Sn<sub>Ga1</sub>) or Sn-on-Ga2 (Sn<sub>Ga2</sub>) defects. Scattering path-lengths up to 3.5  $\text{\AA}$  are considered for fitting the SC sample. For the amorphous thin-film samples, only the first-order peak is fitted by considering Ga–O and Sn–O bonds in the 1NN shell. The non-linear least squares fitting routine is subsequently performed in Artemis to obtain the best-fit parameters. The best-fit parameters for the Sn *K*-edge spectra are included in Table I, while those for the Ga *K*-edge spectra are included as supplementary material in Table SI<sup>15</sup> as many scattering paths are involved. Both  $|\chi(R)|$  and  $k^2$ -weighted  $|\chi(k)|$  spectra are shown in Figures 3 and 4, respectively. However, both the real and imaginary parts of  $\chi(R)$  are included as supplementary material in Figures S3 and S4.<sup>15</sup>

As shown in Figures 3(a) and 4(a), the good agreement between the Ga *K*-edge spectrum for the SC  $\beta$ -Ga<sub>2</sub>O<sub>3</sub>:Sn and our model up to the second order shell corroborates the beta-phase nature of the host lattice as determined using XRD by other authors.<sup>22</sup> By considering two different possibilities in which Sn atoms can be incorporated into the SC  $\beta$ -Ga<sub>2</sub>O<sub>3</sub> host lattice, it is observed that there is a preferential substitution at the Ga2 octahedral site (Sn<sub>Ga2</sub>, *R*-factor = 0.01) as compared to substitution at the Ga1 (Sn<sub>Ga1</sub>, *R*-factor = 0.05). Our observation is also consistent with first-principles calculations by Varley *et al.*<sup>23</sup> Several other studies have also shown that transition metals like In,<sup>24</sup> Cr,<sup>25</sup> and Mn<sup>26</sup> have a preference for the octahedral site and can be explained by steric reasons.<sup>25,26</sup>

For the ALD and PLD amorphous thin-films, the average coordination number to O atoms in Sn's 1NN shell is

TABLE I. Sn *K*-edge EXAFS parameters for all samples. The SC is fitted by assuming either Sn substitution on Ga1 and Ga2 sites. The best fit is obtained for Sn substitution at Ga2 site. Scattering path-lengths up to 3.5 Å are considered for fitting the SC sample.

Site	Shell	Path description	<i>N</i>	<i>R</i> <sub>eff</sub> (Å)	Δ <i>E</i> <sub>0</sub> (eV)	σ <sup>2</sup> (Å <sup>-2</sup> )	R-factor	
SC	Ga1	[Sn1]–O1,1–[Sn1]	1	1.90 (1)	5 (2)	0.000 (2)	0.05	
		[Sn1]–O2,1–[Sn1]	1	1.88 (1)				
		[Sn1]–O3,1–[Sn1]	2	1.84 (1)				
	Ga2	First	[Sn2]–O1,1–[Sn2]	2	1.959 (3)	3.6 (3)	0.0010 (5)	0.01
			[Sn2]–O2,1–[Sn2]	1	1.996 (3)			
			[Sn2]–O2,2–[Sn2]	2	2.062 (3)			
			[Sn2]–O3,1–[Sn2]	1	1.940 (3)			
			[Sn2]–Ga1,1–[Sn2]	1	3.37 (2)			
		Second	[Sn2]–Ga1,2–[Sn2]	2	3.42 (2)			
			[Sn2]–Ga1,3–[Sn2]	2	3.47 (2)			
			[Sn2]–Ga1,4–[Sn2]	2	3.55 (2)			
			[Sn2]–Ga2,1–[Sn2]	2	3.06 (1)			
			[Sn2]–Ga2,2–[Sn2]	2	3.09 (1)			
			[Sn2]–O1,2–[Sn2]	1	3.34 (6)	0.02 (1)		
			[Sn2]–O1,3–[Sn2]	1	3.48 (6)			
			[Sn2]–O2,3–[Sn2]	2	3.63 (6)			
			[Sn2]–O3,2–[Sn2]	1	3.42 (6)			
			[Sn2]–O3,3–[Sn2]	1	3.34 (6)			
			[Sn2]–O3,4–[Sn2]	2	3.46 (6)			
ALD	First	[Sn]–O3,1–[Sn]	5.0 (2)	2.030 (3)	4.4 (3)	0.0076 (6)	0.005	
PLD	First	[Sn]–O3,1–[Sn]	5.1 (2)	2.117 (4)	8.2 (3)	0.0128 (8)	0.008	

found to be close to 5.0, despite the difference in charge state of the central absorbing Sn atoms. This suggests that our amorphous films might not be deposited in thermodynamic equilibrium conditions, because Sn atoms in SnO<sub>2</sub> (Sn<sup>4+</sup>) and SnO (Sn<sup>2+</sup>) tend to favor octahedral and tetrahedral coordination, respectively. Despite similar coordination numbers, the larger Sn<sup>2+</sup> ions in the PLD thin-film increases the average Sn–O bond-length (*R*<sub>eff</sub> = 2.117 Å) as well as the structural disorder (σ<sup>2</sup> = 0.0128 Å<sup>-2</sup>) relative to the ALD

films (*R*<sub>eff</sub> = 2.030 Å and σ<sup>2</sup> = 0.0076 Å<sup>-2</sup>). The lack of long range order in both ALD and PLD thin-films suggests that a non-crystalline structure could represent an impediment for dopant activation. One further explanation for the ALD thin-film to exhibit low conductivity despite the presence of Sn<sup>4+</sup> could be the formation of a compensating defect in the that reduces the number of “activated” Sn<sup>4+</sup>; such a phenomenon has been observed in crystalline ZnO:Ga.<sup>27</sup> Lastly, post-annealing has been performed in this work in an attempt to activate the dopants in ALD Ga<sub>2</sub>O<sub>3</sub>:Sn thin-films (1 h in N<sub>2</sub> atmosphere at 1000 °C). However, both the film resistivity and crystalline order did not exhibit any detectable change, and the authors are of the opinion that it might be necessary to anneal the films beyond 1000 °C to achieve crystalline Ga<sub>2</sub>O<sub>3</sub> for dopant activation.

In conclusion, XAS is used to investigate the differences in the local structures of conductive single-crystal β-Ga<sub>2</sub>O<sub>3</sub>:Sn and resistive a-Ga<sub>2</sub>O<sub>3</sub>:Sn thin-films. Our results can be used to help engineer Ga<sub>2</sub>O<sub>3</sub>:Sn thin-films with the favorable electrical properties of single crystal β-Ga<sub>2</sub>O<sub>3</sub>:Sn. Our XAS analyses indicate that activated Sn dopant atoms in conductive single-crystal β-Ga<sub>2</sub>O<sub>3</sub>:Sn are present as Sn<sup>4+</sup>, which preferentially substitutes for Ga at the octahedral Ga2 site as predicted by previous theoretical calculations. On the other hand, inactive Sn dopants in resistive a-Ga<sub>2</sub>O<sub>3</sub> are present in either +2 or +4 charge states, depending on growth conditions. Lastly, XAS results indicate a lack of structural order beyond the 1NN shell in a-Ga<sub>2</sub>O<sub>3</sub> samples, which suggests that a crystalline structure might be necessary for high dopant activation. Consequently, both achieving crystalline Ga<sub>2</sub>O<sub>3</sub> and controlling the oxidation state of Sn during growth appear to be necessary to obtain high Ga<sub>2</sub>O<sub>3</sub> conductivity.

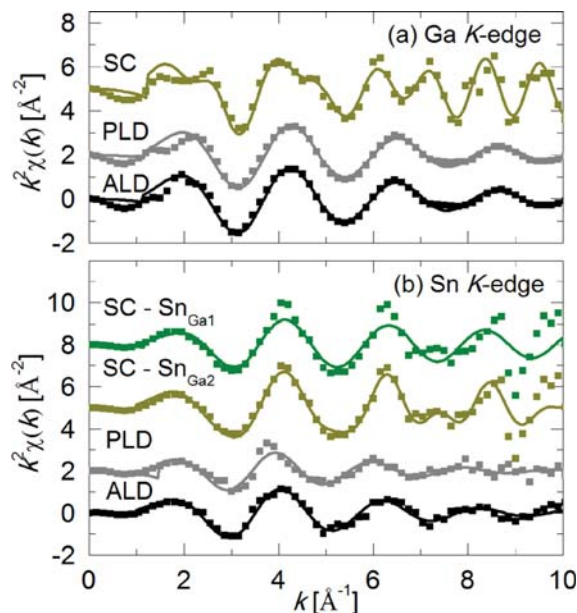


FIG. 4. *k*<sup>2</sup>-weighted EXAFS spectra for (a) Ga and (b) Sn *K*-edges. Fits to both the Sn<sub>Ga1</sub> and Sn<sub>Ga2</sub> for the SC sample are shown in (b).

This work was supported as part of the Center for Next Generation Materials by Design (CMGMD), an Energy Frontier Research Center funded by the U.S. Department of Energy, Office of Science, Basic Energy Sciences under Contract No. DE-AC36-08GO28308. Use of the Stanford Synchrotron Radiation Lightsource, SLAC National Accelerator Laboratory, was supported by the U.S. Department of Energy, Office of Basic Energy Sciences under Contract No. DE-AC02-76SF00515. Use of the Advanced Photon Source at Argonne National Laboratory was supported by the U.S. Department of Energy, Office of Science, Office of Basic Energy Sciences, under Contract No. DE-AC02-06CH11357. MRCAT operations are supported by the Department of Energy and the MRCAT member institutions. S. Lany, D. S. Ginley, W. Tumas (NREL), and A. M. Kolpak (MIT) are thanked for helpful discussions. J.R. Poindexter (MIT) is thanked for synchrotron assistance. S.C.S., R.E.B., K.L., and R.J. acknowledge a Clean Energy Scholarship from NRF Singapore, an NSF Graduate Research Fellowship, a Kwanjeong Education Foundation Fellowship, and a U.S. Department of Energy EERE Postdoctoral Research Award, respectively. Lastly, Tamura Corporation is thanked for providing insightful information.

S.C.S., R.E.B., R.J., and T.B. designed the experiment; M.D.H. and D.C. fabricated the PLD and ALD samples, respectively; S.C.S. performed Hall; J.D.P. performed RBS; L.S. performed XRD at SLAC; S.C.S., R.E.B., R.J., T.B., L.S., K.L., J.W., and C.U.S. acquired XAS data; S.C.S. fitted the XAS data; S.C.S. wrote the paper; R.G.G., M.T., and T.B. supervised the research. All authors reviewed and commented on the manuscript.

- <sup>1</sup>T. S. Lay, M. Hong, J. Kwo, J. P. Mannaerts, W. H. Hung, and D. J. Huang, *Solid State Electron.* **45**, 1679 (2001).
- <sup>2</sup>E. G. Villora, K. Shimamura, Y. Yoshikawa, T. Ujiie, and K. Aoki, *Appl. Phys. Lett.* **92**, 202120 (2008).
- <sup>3</sup>N. Suzuki, S. Ohira, M. Tanaka, T. Sugawara, K. Nakajima, and T. Shishido, *Phys. Status Solidi C* **4**, 2310 (2007).
- <sup>4</sup>M. Higashiwaki, K. Sasaki, A. Kuramata, T. Masui, and S. Yamakoshi, *Phys. Status Solidi A* **211**, 21 (2014).
- <sup>5</sup>T. Minami, Y. Nishi, and T. Miyata, *Appl. Phys. Express* **6**, 044101 (2013).

- <sup>6</sup>Y. S. Lee, D. Chua, R. E. Brandt, S. C. Siah, J. V. Li, J. P. Mailoa, S. W. Lee, R. G. Gordon, and T. Buonassisi, *Adv. Mater.* **26**, 4704 (2014).
- <sup>7</sup>T. G. Allen and A. Cuevas, *Appl. Phys. Lett.* **105**, 031601 (2014).
- <sup>8</sup>M. Fleischer and H. Meixner, *Sens. Actuators, B* **4**, 437 (1991).
- <sup>9</sup>E. Nogales, J. A. García, B. Méndez, J. Piqueras, K. Lorenz, and E. Alves, *J. Phys. D: Appl. Phys.* **41**, 065406 (2008).
- <sup>10</sup>D. J. Comstock and J. W. Elam, *Chem. Mater.* **24**, 4011 (2012).
- <sup>11</sup>K. Sasaki, A. Kuramata, T. Masui, E. G. Villora, K. Shimamura, and S. Yamakoshi, *Appl. Phys. Express* **5**, 035502 (2012).
- <sup>12</sup>B. K. Newman, E. Ertekin, J. T. Sullivan, M. T. Winkler, M. A. Marcus, S. C. Fakra, M.-J. Sher, E. Mazur, J. C. Grossman, and T. Buonassisi, *J. Appl. Phys.* **114**, 133507 (2013).
- <sup>13</sup>S. C. Siah, R. Jaramillo, R. Chakraborty, P. T. Erslev, C. Sun, T. Weng, M. F. Toney, G. Teeter, and T. Buonassisi, *IEEE J. Photovoltaics* **5**, 372 (2014).
- <sup>14</sup>S. C. Siah, S. W. Lee, Y. S. Lee, J. Heo, T. Shibata, C. U. Segre, R. G. Gordon, and T. Buonassisi, *Appl. Phys. Lett.* **104**, 242113 (2014).
- <sup>15</sup>See supplementary material at <http://dx.doi.org/10.1063/1.4938123> for full Sn *K*-edge XANES spectra, XRD measurements, Ga *K*-edge EXAFS parameters, magnitude and real part of the fitted Fourier-transformed EXAFS spectra for Ga and Sn *K*-edges and magnitude and imaginary part of the fitted Fourier-transformed EXAFS spectra for Ga and Sn *K*-edges.
- <sup>16</sup>L. Qiao, H. Y. Xiao, S. M. Heald, M. E. Bowden, T. Varga, G. J. Exarhos, M. D. Biegalski, I. N. Ivanov, W. J. Weber, T. C. Droubay, and S. A. Chambers, *J. Mater. Chem. C* **1**, 4527 (2013).
- <sup>17</sup>D. C. Koningsberger and R. Prins, *X-Ray Absorption: Principles, Applications, Techniques of EXAFS, SEXAFS, and XANES* (Blackwell Scientific Publications, Eindhoven, The Netherlands, 1988).
- <sup>18</sup>P. Villars, *Material Phases Data System (MPDS)* (CH-6354 Vitznau, Switzerland, 2014).
- <sup>19</sup>S. Grindy, B. Meredig, S. Kirklín, J. E. Saal, and C. Wolverton, *Phys. Rev. B* **87**, 075150 (2013).
- <sup>20</sup>B. Ravel and M. Newville, *J. Synchrotron Radiat.* **12**, 537 (2005).
- <sup>21</sup>T. C. Lovejoy, R. Chen, E. N. Yitamben, V. Shutthanadan, S. M. Heald, E. G. Villora, K. Shimamura, S. Zheng, S. T. Dunham, F. S. Ohuchi, and M. A. Olmstead, *J. Appl. Phys.* **111**, 123716 (2012).
- <sup>22</sup>E. G. Villora, S. Arjoca, K. Shimamura, D. Inomata, and K. Aoki, *Proc. SPIE*, **8987**, 89871U (2014).
- <sup>23</sup>J. B. Varley, J. R. Weber, A. Janotti, and C. G. Van de Walle, *Appl. Phys. Lett.* **97**, 142106 (2010).
- <sup>24</sup>M. B. Maccioni, F. Ricci, and V. Fiorentini, *Appl. Phys. Express* **8**, 021102 (2015).
- <sup>25</sup>T. H. Yeom, I. G. Kim, S. H. Lee, S. H. Choh, and Y. M. Yu, *J. Appl. Phys.* **93**, 3315 (2003).
- <sup>26</sup>I. G. Kim, T. H. Yeom, S. H. Lee, Y. M. Yu, H. W. Shin, and S. H. Choh, *J. Appl. Phys.* **89**, 4470 (2001).
- <sup>27</sup>A. Zakutayev, N. H. Perry, T. O. Mason, D. S. Ginley, and S. Lany, *Appl. Phys. Lett.* **103**, 232106 (2013).